Computed tomography-based radiomics decodes prognostic and molecular differences in interstitial lung disease related to systemic sclerosis

Janine Schniering [1,2], Malgorzata Maciukiewicz[1], Hubert S. Gabrys[3], Matthias Brunner[1,4], Christian Blüthgen[5], Chantal Meier[1], Sophie Braga-Lagache[6], Anne-Christine Uldry[6], Manfred Heller[6], Matthias Guckenberger[3], Håvard Fretheim[7], Christos T. Nakas [8,9], Anna-Maria Hoffmann-Vold[7], Oliver Distler[1], Thomas Frauenfelder[5], Stephanie Tanadini-Lang [3] and Britta Maurer [1,4]

[1]Center of Experimental Rheumatology, Dept of Rheumatology, University Hospital Zurich, University of Zurich, Zurich, Switzerland. [2]Institute of Lung Biology and Disease and Comprehensive Pneumology Center, Helmholtz Zentrum München, Member of the German Center for Lung Research (DZL), Munich, Germany. [3]Dept of Radiation Oncology, University Hospital Zurich, University of Zurich, Zurich, Switzerland. [4]Dept of Rheumatology and Immunology, University Hospital Bern, University Bern, Bern, Switzerland. [5]Institute of Diagnostic and Interventional Radiology, University Hospital Zurich, University of Zurich, Zurich, Switzerland. [6]Proteomics and Mass Spectrometry Core Facility, Dept for BioMedical Research (DBMR), University of Bern, Bern, Switzerland. [7]Dept of Rheumatology, Oslo University Hospital and Institute of Clinical Medicine, University of Oslo, Oslo, Norway. [8]Laboratory of Biometry, University of Thessaly, Volos, Greece. [9]University Institute of Clinical Chemistry, Inselspital, Bern University Hospital, University of Bern, Bern, Switzerland.

Corresponding author: Britta Maurer (britta.maurer@insel.ch)

Shareable abstract (@ERSpublications)
CT-based radiomics decodes phenotypic, prognostic and molecular differences in SSc-ILD, and predicts progression-free survival with a significant impact on future clinical decision making in SSc-ILD https://bit.ly/3zPaMOn

Cite this article as: Schniering J, Maciukiewicz M, Gabrys HS, *et al*. Computed tomography-based radiomics decodes prognostic and molecular differences in interstitial lung disease related to systemic sclerosis. *Eur Respir J* 2022; 59: 2004503 [DOI: 10.1183/13993003.04503-2020].

Received: 12 Dec 2020
Accepted: 23 Sept 2021

Abstract

Background Radiomic features calculated from routine medical images show great potential for personalised medicine in cancer. Patients with systemic sclerosis (SSc), a rare, multiorgan autoimmune disorder, have a similarly poor prognosis due to interstitial lung disease (ILD). Here, our objectives were to explore computed tomography (CT)-based high-dimensional image analysis ("radiomics") for disease characterisation, risk stratification and relaying information on lung pathophysiology in SSc-ILD.

Methods We investigated two independent, prospectively followed SSc-ILD cohorts (Zurich, derivation cohort, n=90; Oslo, validation cohort, n=66). For every subject, we defined 1355 robust radiomic features from standard-of-care CT images. We performed unsupervised clustering to identify and characterise imaging-based patient clusters. A clinically applicable prognostic quantitative radiomic risk score (qRISSc) for progression-free survival (PFS) was derived from radiomic profiles using supervised analysis. The biological basis of qRISSc was assessed in a cross-species approach by correlation with lung proteomic, histological and gene expression data derived from mice with bleomycin-induced lung fibrosis.

Results Radiomic profiling identified two clinically and prognostically distinct SSc-ILD patient clusters. To evaluate the clinical applicability, we derived and externally validated a binary, quantitative radiomic risk score (qRISSc) composed of 26 features that accurately predicted PFS and significantly improved upon clinical risk stratification parameters in multivariable Cox regression analyses in the pooled cohorts. A high qRISSc score, which identifies patients at risk for progression, was reverse translatable from human to experimental ILD and correlated with fibrotic pathway activation.

Conclusions Radiomics-based risk stratification using routine CT images provides complementary phenotypic, clinical and prognostic information significantly impacting clinical decision making in SSc-ILD.

Introduction

Despite the emergence of targeted therapies, interstitial lung disease (ILD), the leading cause of death in systemic sclerosis (SSc), remains a key challenge due to the high variability in patient-specific disease

trajectories and progression rates [1]. This high interindividual variability warrants valid prognostic biomarkers for individual risk stratification and personalised management, which so far are lacking [2]. Traditionally, molecular data from tissue biopsies have been explored for precision medicine strategies. However, the invasiveness of tissue biopsies, the unsuitability for longitudinal assessments, the high risk of nonrepresentative sampling due to spatial disease heterogeneity and the high costs associated with molecular profiling have mostly limited clinical implementation. This applies even more to SSc-ILD, where lung biopsies are only exceptionally performed since they are not required for diagnosis [3]. Medical imaging, particularly high-resolution computed tomography (HRCT), is an integral part of the standard of care of SSc-ILD, as it allows both diagnosis and longitudinal monitoring of the entire lung pathology with high sensitivity [4–6].

Recently, high-dimensional image analysis, termed "radiomics", has opened novel avenues for imaging-based disease subtyping and outcome prediction [7–10]. Radiomic features are computationally retrieved, quantitative data derived from medical images which describe the tissue in terms of its intensity, texture and advanced statistical properties [11]. Their unique and added value compared with visual or other quantitative imaging methodologies [12–14] lies in the ability to capture tissue phenotypes on different spatial scales ranging from the radiological/macroscopic to the molecular/microscopic level [8, 10, 15], which adds another dimension. Thereby, they provide novel and complementary information compared with clinical reports, laboratory and functional tests.

To address the high, unmet need for validated risk parameters, here we explored the potential of HRCT-based radiomics for disease characterisation and outcome prediction in SSc-ILD.

Methods

A detailed description of the methods is provided in the supplementary material.

Study design and datasets

We retrospectively investigated two independent prospectively followed cohorts of SSc-ILD including 90 patients (76.7% female, median age 57.5 years) from University Hospital Zurich, Zurich, Switzerland (derivation cohort) and 66 patients (75.8% female, median age 61.0 years) from Oslo University Hospital, Oslo, Norway (validation cohort). All included patients met the following criteria: diagnosis of SSc according to the Very Early Diagnosis of Systemic Sclerosis (VEDOSS) study [16] or the 2013 American College of Rheumatology/European League against Rheumatism classification criteria [17], presence of ILD on HRCT and availability of a HRCT scan fulfilling the predefined quality criteria (supplementary material). A summary of patient demographics and clinical characteristics at baseline for both study cohorts is given in table 1.

A third dataset derived from an experimental cohort of 30 mice with bleomycin-induced lung fibrosis, a widely acknowledged pre-clinical model for ILD [19], was used for correlation studies with biological features, including proteomic, histological and gene expression data. For every subject, we defined and extracted 1386 radiomic features (Excel file in the supplementary material) from semiautomated segmented HRCT images, including 17 intensity, 137 texture and 1232 wavelet features, using our in-house-developed radiomics software Z-Rad. A detailed description of the study workflow is available in figure 1. The local ethics committees approved the study (approvals pre-BASEC-EK-839 (KEK 2016-01515), KEK-ZH 2010-158/5, BASEC 2018-02165 and BASEC 2018-01873) and written informed consent was obtained from every patient.

Statistical analyses

Robustness of radiomic features against semiautomated lung delineation was assessed by intra- and inter-reader intraclass correlation (ICC) analysis, and unstable features (ICC <0.75) were excluded from further analyses, resulting in a final set of 1355 robust radiomic features (supplementary figure S1). Unsupervised *k*-means clustering was performed to identify homogeneous imaging-based patient clusters without *a priori* assumptions in the derivation cohort (Zurich; n=90). Next, a quantitative composite radiomic risk score (qRISSc) for progression-free survival (PFS) was built to evaluate the clinical applicability. PFS was defined as the time from the date of the HRCT to the date of the first occurrence of ILD progression (relative decline in forced vital capacity (FVC) % pred ⩾15%). qRISSc, composed of 26 features, was derived by two-step feature selection, including univariable Cox regression and cross-validated LASSO (least absolute shrinkage and selection operator) penalised regression, and was further developed into a binary score with an optimal cut-off value of 0.21. Associations with clinical characteristics and PFS among the obtained patient clusters and qRISSc-based risk groups were assessed by Fisher's exact test and the Mann–Whitney U-test or univariable Cox regression, respectively.

TABLE 1 Summary of patient demographics and clinical characteristics for the two patient cohorts included in this study

	Zurich cohort (n=90)	Oslo cohort (n=66)	p-value
Age (years)	57.5±17.8	61.0±18.8	0.641
Sex			
Male	21 (23.3)	16 (24.2)	1.000
Female	69 (76.7)	50 (75.8)	
SSc disease duration (years)[#]	5.0±8.2	5.3±9.2	0.874
SSc subset [18]			
Limited cutaneous SSc	41 (45.6)	37 (56.1)	0.041*
Diffuse cutaneous SSc	42 (46.7)	29 (43.9)	
No skin involvement	7 (7.8)	0 (0.0)	
Skin involvement			
Limited cutaneous	31 (34.4)	37 (56.1)	<0.001*
Diffuse cutaneous	43 (47.8)	29 (43.9)	
No skin involvement	9 (10.0)	0 (0.0)	
Only sclerodactyly	7 (7.8)	0 (0.0)	
Autoantibodies			
Anti-centromere positive	13 (14.4)	7 (10.6)	1.000
Anti-topoisomerase 1 positive	41 (45.6)	24 (36.4)	0.614
Anti-RNA polymerase III positive	7 (7.8)	8 (12.1)	0.261
Anti-PM/Scl positive	18 (20.0)	4 (6.1)	0.032*
FVC (% pred)	87.5±33.9	85.0±36.0	0.605
⩾70% pred	64 (71.1)	44 (66.7)	0.851
<70% pred	24 (26.7)	15 (22.7)	
D_{LCO} (% pred)	66.5±29.4	61.0±29.0	0.078
FEV_1 (% pred)	88.7±31.2	77.0±26.5	0.088
Pulmonary hypertension[¶]	20 (22.2)	6 (9.1)	0.048*
PAPsys (mmHg)[+]	26.0±10.0	21.0±20.0	0.028*
CRP ($mg \cdot L^{-1}$)	3.1±5.6	3.6±8.0	0.259
6-min walk distance (m)	511.0±161.0	NA	NA
S_{pO_2} before 6MWT (%)	96.0±2.0	NA	NA
S_{pO_2} after 6MWT (%)	95.0±7.0	NA	NA
Borg scale (range 0–10)	3.0±2.0	NA	NA
Extent of lung fibrosis on HRCT			
<20%	50 (55.6)	30 (45.5)	0.257
⩾20%	40 (44.4)	36 (54.5)	
Ground-glass opacification	45 (50.0)	42 (63.6)	0.104
Reticular changes	87 (96.7)	51 (77.3)	<0.001*
Traction bronchiectasis	50 (55.6)	27 (40.9)	0.077
Honeycombing	22 (24.4)	16 (24.2)	1.000
Bullae	3 (3.3)	4 (6.1)	0.457
Radiological subtype			
NSIP	49 (54.4)	34 (51.5)	0.602
UIP[§]	37 (41.1)	27 (40.9)	
DIP	1 (1.1)	0 (0.0)	
Unclassifiable	3 (3.3)	5 (7.6)	
Immunomodulatory therapy[ƒ]	51 (56.7)	28 (42.4)	0.105
Smoking status			
Never-smoker	55 (61.1)	24 (36.4)	0.025*
Ex-smoker	21 (23.3)	25 (37.9)	
Current smoker	12 (13.3)	5 (7.6)	
Died during follow-up[##]	20 (22.2)	22 (33.3)	0.009*
Relative FVC decline ⩾15% during follow-up	27 (30.0)	11 (16.7)	0.113
Visual HRCT progression during follow-up	21 (23.3)	18 (27.3)	0.316

Data are presented as median±interquartile range or n (%), unless otherwise stated. SSc: systemic sclerosis; FVC: forced vital capacity; D_{LCO}: diffusing capacity of the lung for carbon monoxide; FEV_1: forced expiratory volume in 1 s; PAPsys: systolic pulmonary arterial pressure; CRP: C-reactive protein; NA: not available; S_{pO_2}: peripheral oxygen saturation; 6MWT: 6-min walk test; HRCT: high-resolution computed tomography; NSIP: nonspecific interstitial pneumonia; UIP: usual interstitial pneumonia; DIP: diffuse interstitial pneumonia. [#]: disease duration of SSc was calculated as the difference between the date of baseline CT and the date of manifestation of the first non-Raynaud's symptom; [¶]: pulmonary hypertension was assessed by echocardiography or right heart catheterisation; [+]: PAPsys was determined by right heart catheterisation; [§]: UIP includes the radiological diagnosis of both "definite" and "probable" UIP; [ƒ]: immunomodulatory therapy included prednisone, methotrexate, rituximab, cyclophosphamide, mycophenolate mofetil, hydroxychloroquine, tocilizumab, imatinib, azathioprine, adalimumab, leflunomide and cyclosporine; [##]: cause of death included SSc-associated interstitial lung disease, pulmonary arterial hypertension, viral pneumonia, pulmonary embolism, septic shock, brain haemorrhage, caecal cancer, pancreatic carcinoma and lung cancer. p-values of univariate comparisons of baseline characteristics between the two cohorts are shown. Fisher's exact test was used to compare categorical variables and the Mann–Whitney U-test was used to compare continuous variables. *: p<0.05.

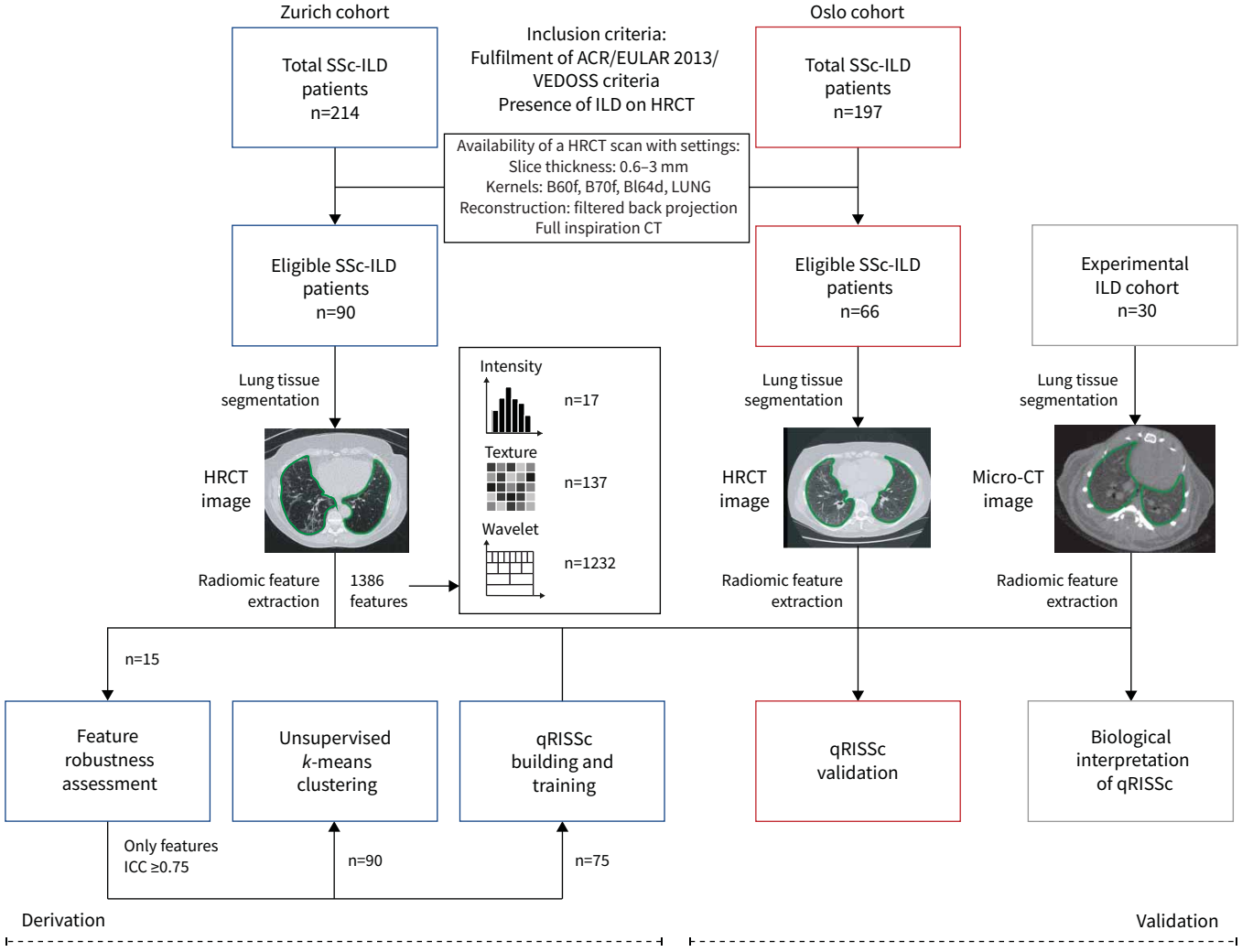

FIGURE 1 Study workflow. We applied radiomics to three different datasets, including two independent cohorts of systemic sclerosis-associated interstitial lung disease (SSc-ILD) patients from University Hospital Zurich (derivation cohort) and Oslo University Hospital (validation cohort), and one experimental ILD cohort composed of 30 bleomycin-treated mice for association studies with biological features (*i.e.* proteomic, histological and gene expression data). Patients were retrospectively selected based on the fulfilment of early/mild SSc according to the Very Early Diagnosis of Systemic Sclerosis (VEDOSS) criteria [16] or established disease according to the 2013 American College of Rheumatology/European League against Rheumatism (ACR/EULAR) classification criteria [17], presence of ILD on high-resolution computed tomography (HRCT) as determined by a senior radiologist and predefined quality criteria for their HRCT images. For every subject, in total, 1386 radiomic features were extracted from semiautomated segmented CT images, including 17 intensity, 137 texture and 1232 wavelet features, using our in-house-developed software Z-Rad. Filtering of robust radiomic features (intraclass correlation (ICC) ⩾0.75), unsupervised clustering and construction of the quantitative radiomic ILD risk score (qRISSc) for progression-free survival in SSc-ILD were performed in the Zurich cohort. Independent and external validation of the qRISSc was performed using the Oslo cohort.

Multivariable Cox regression analyses with hazards ratio (HR) and 95% confidence interval and C-index were applied to analyse the predictive ability of conventional clinical risk factors and qRISSc for progressive ILD in the pooled cohorts (n=156). The C-index is equivalent to the area under the curve in receiver operating characteristic curve analysis and can be used in Cox regression analysis [20]. Spearman correlation analysis with histological, gene expression and whole-lung proteomic data obtained from mice with bleomycin-induced lung fibrosis and pathway enrichment analysis was performed to define the biological basis of qRISSc.

Results

Radiomic profiling captures clinical and prognostic differences among SSc-ILD patients

In a first discovery approach, we explored the radiomic phenotypes of the 90 SSc-ILD patients from the Zurich cohort with unsupervised clustering and examined their associations with clinical characteristics and

patient outcome among the obtained clusters. Clustering of the 1355 robust radiomic features revealed two distinct and stable patient clusters based on their radiomic profiles (Jaccard coefficients of 0.90 and 0.82 for clusters 1 and 2, respectively, where 1 indicates perfect stability) (figure 2a and b). The differences in clinical characteristics were substantial (figure 2 and supplementary table S1), with patients in cluster 2 (n=31) having a significantly more impaired lung function ($p<0.001$) (figure 2c), worse performance in the 6-min walk test (figure 2c) and a higher frequency of pulmonary hypertension ($p=0.001$) (figure 2a and c) than patients in cluster 1 (n=59). Cluster 2 was also significantly enriched for honeycombing ($p=0.009$) as a radiological sign of more severe fibrotic lung remodelling.

Most notably, radiomic clusters did not stratify patients according to classical definitions of ILD severity, including limited and extensive disease extent as defined by HRCT analysis (HRCT threshold <20% or ⩾20%) or pulmonary function tests (FVC ⩾70% or <70%) [21], respectively. However, significant associations with both disease classifiers were detected ($p=0.002$ and $p<0.001$, respectively).

Furthermore, the clusters did not differ in common SSc clinical, demographic and serological characteristics, including age, sex, SSc disease duration, active immunomodulatory therapy, extent of skin involvement, autoantibody profiles or C-reactive protein (CRP) levels [17, 22] (figure 2a and c and supplementary table S1).

We next assessed whether the patients of the two clusters also differed in their outcome by survival analysis with the Kaplan–Meier estimator. Consistent with their worse disease phenotype, patients in cluster 2 showed a higher probability of faster disease progression and a decrease in PFS defined by either the time to relative decline of ⩾15% in FVC % pred ($p=0.001$; HR 3.52, 95% CI 1.66–7.45) (figure 2d) or the time to decline assessed by a recently proposed FVC–diffusing capacity of the lung for carbon monoxide (D_{LCO}) composite index [22] ($p=0.005$; HR 2.73, 95% CI 1.36–5.50) (figure 2e). In addition, a marginal association with time to visual disease progression on HRCT ($p=0.102$) and overall survival ($p=0.104$) was detected, suggesting a higher risk for visual ILD progression and all-cause death for patients in cluster 2 (figure 2f and g).

Collectively, this exploratory analysis demonstrated that HRCT-based radiomic profiling captured clinical and prognostic differences in SSc-ILD that were complementary to the information provided by routine clinical, functional and imaging tests.

A clinically applicable radiomic risk score predicts PFS in SSc-ILD and improves upon existing stratification parameters

Having found that radiomic features identified prognostically distinct SSc-ILD patient clusters, we next assessed the clinical applicability of radiomics for outcome prediction.

To that end, we derived a prognostic composite radiomic signature as recently proposed by Lu *et al.* [10] for risk stratification in ovarian cancer using the Zurich cohort as a derivation cohort. The resulting quantitative radiomic risk score for PFS, qRISSc, comprising 26 radiomic features (n=4 intensity, n=9 texture and n=13 wavelet features) (supplementary table S2), accurately stratified patients according to their risk for future lung decline with an optimal cut-off value of 0.21. In the derivation cohort (Zurich), high-risk patients had a higher probability of earlier lung function decline than low-risk patients (median PFS time 48.0 *versus* 82.30 months) (figure 3a). Most importantly, the final, binary version of qRISSc for risk stratification was independently confirmed. In the external validation cohort from Oslo, qRISSc-identified high-risk patients were at significant risk for progression (HR 5.14, 95% CI 14–23.20), with a median PFS time of 41.7 months compared with 88 months in the low-risk group ($p=0.03$) (figure 3b).

Similarly to what was previously shown for the two distinct radiomic patient clusters, qRISSc-stratified high- and low-risk patient groups differed in their clinical characteristics (figure 3c and supplementary tables S3 and S4). High-risk patients consistently presented with worse lung function parameters and showed an association with the presence of pulmonary hypertension, the extent of fibrosis on HRCT and specific visual ILD HRCT patterns, including honeycombing and traction bronchiectasis (figure 3c).

Next, we evaluated whether qRISSc improved upon previously proposed clinical risk factors for SSc-ILD progression, including age, sex, baseline FVC and D_{LCO}, disease extent on HRCT, radiological subtype, SSc subtype, autoantibody status and CRP [23–30] in both univariable and multivariable Cox regression analysis.

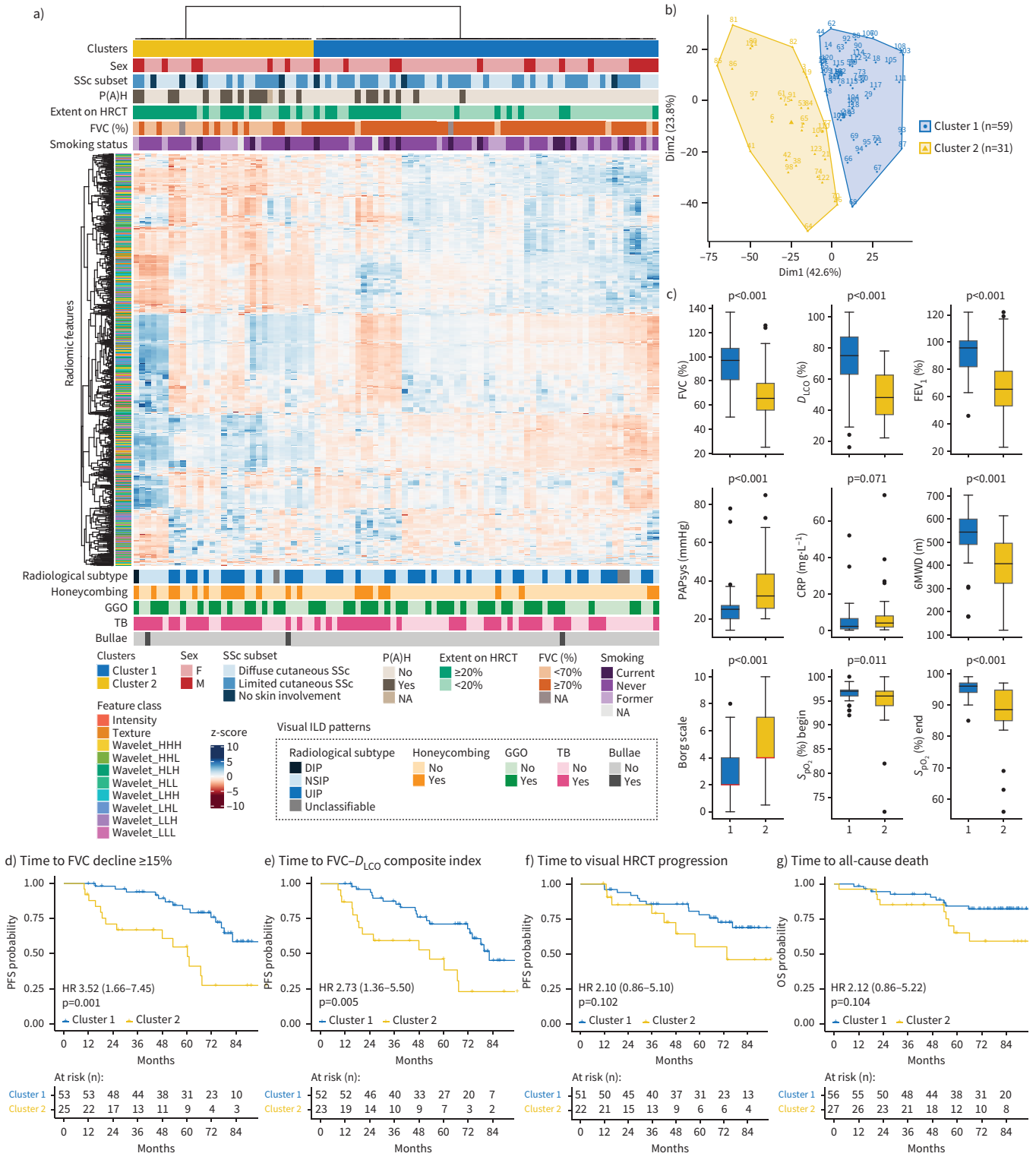

FIGURE 2 Unsupervised *k*-means clustering of radiomic data from systemic sclerosis-associated interstitial lung disease (SSc-ILD) patients. a) Heatmap summarising the *k*-means clustering results (Zurich cohort, n=90). Before clustering, radiomic features were z-scored. Associations between the two identified radiomic patient clusters with categorical clinical parameters (top) and visual ILD patterns depicted on high-resolution computed tomography (HRCT) (bottom) are shown. b) *k*-means cluster plot indicating two stable clusters (Jaccard coefficient for cluster 1 (blue) 0.90 and for cluster 2 (yellow) 0.82, where 1 indicates perfect stability). c) Top row: box plots comparing lung function parameters between clusters 1 and 2 (forced vital capacity (FVC) % pred, diffusing capacity of the lung for oxygen (D_{LCO}) % pred and forced expiratory volume in 1 s (FEV_1) % pred); middle row: box plots showing systolic pulmonary arterial pressure (PAPsys), C-reactive protein (CRP) and 6-min walk distance (6MWD) for

both clusters; bottom row: box plots indicating the Borg scale of perceived exertion (scale 0–10: 0=no exertion, 1=very weak, 2=weak, 3=moderate, 5=strong, 7=very strong, 10=extreme exertion) and peripheral oxygen saturation (S_{pO_2}) at the beginning and end of the test per patient cluster. d–f) Kaplan–Meier curves for progression-free survival (PFS) defined as either d) time to relative FVC decline ⩾15%, e) time to FVC–D_{LCO} composite index (relative decrease in FVC % pred of ⩾15%, or a relative decline in FVC % pred of ⩾10% combined with D_{LCO} % pred of ⩾15% according to [22]) or f) time to visual ILD progression on HRCT. g) Kaplan–Meier plot for overall survival (OS) defined as time to all-cause death. Hazard ratio (95% CI) and p-value of the univariate Cox regression are shown. P(A)H: pulmonary (arterial) hypertension; F: female; M: male; NA: not available; DIP: diffuse interstitial pneumonia; NSIP: nonspecific interstitial pneumonia; UIP: usual interstitial pneumonia; GGO: ground-glass opacification; TB: traction bronchiectasis.

The univariable analysis only revealed baseline D_{LCO} apart from qRISSc to be significantly and consistently associated with PFS among the two study cohorts (figure 4a), yet with significantly weaker hazard ratios (HR 0.95–0.97; p<0.05) than qRISSc (HR 4.07–5.14; p<0.05) (supplementary table S5).

In multivariable Cox regression analysis of the pooled cohorts, the integration of qRISSc into models composed of different combinations of the clinically pertinent risk factors for SSc-ILD progression significantly improved the power of outcome prediction as measured by the C-index (figure 4b and supplementary figure S2b) compared with the models exclusively composed of the clinical risk factors (supplementary tables S6–S8). In addition, in multivariable analysis, as in univariate analysis, qRISSc remained the strongest (HR 3.07–4.23) and often the only significant predictor in the combined models (figure 4c, supplementary figure S2a and supplementary tables S7 and S8).

Of note, in the pooled study cohorts, qRISSc was shown to be also associated with other clinically used definitions of ILD progression, including different thresholds of FVC decline (*i.e.* absolute FVC decline of ⩾10% or ⩾15% or relative FVC decline of ⩾5% or ⩾10%; p<0.05) (supplementary figure S3b–e), the FVC–D_{LCO} composite index (p<0.001) (supplementary figure S3a–f), visual ILD progression on HRCT (p=0.031) (supplementary figure S3b–g) and overall survival (p<0.001) (supplementary figure S3c–h). No significant association of qRISSc was found with an absolute FVC decline of 5% (p=0.16) (supplementary figure S3a).

Furthermore, we compared the prognostic performance of qRISSc to a quantitative score only composed of less complex, first-order densitometric (intensity) features that were used in the past to quantify disease extent and progression in SSc-ILD [31–34]. While the intensity score was prognostic for future lung function decline in the derivation cohort (p=0.004), it was not significant in the external validation cohort (p=0.08), thus showing that the consideration of more abstract radiomic features provides additional important prognostic information (supplementary figure S4).

The clinical applicability of qRISSc was further confirmed by demonstrating that radiomic features, including qRISSc features, did not separate patients according to different imaging sites and settings employed in Zurich *versus* Oslo (supplementary figure S5 and supplementary table S9) [35].

In summary, our newly derived binary radiomic risk score, qRISSc, accurately predicted PFS and significantly improved upon conventional risk stratification tools in two independent cohorts of SSc-ILD.

The quantitative radiomic risk score is associated with fibrotic pathway activation on a molecular level

The added and complementary value of radiomic profiling might ultimately arise from the integrated in-depth analysis of tissue heterogeneity over the spatial spectrum from the radiological/macroscopic to the molecular/microscopic level, covering pathological information of the whole organ [36]. Therefore, we next assessed the association of qRISSc with specific pathophysiological processes to define the biological underpinning for the stratification into high- and low-risk patients.

Since lung biopsies are only rarely performed in SSc-ILD [3] and consequently imaging-matched human biosamples were not available, we used a cross-species correlation approach, employing the mouse model of bleomycin-induced lung fibrosis as a model system for SSc-ILD. For this model, we have recently confirmed that radiomic signatures largely translate between experimental ILD in bleomycin-treated mice and ILD in SSc patients [37].

We first compared qRISSc values obtained in mice and our two patient cohorts to ensure that qRISSc reverse translates from patients to mice. We found a very similar score distribution between all three

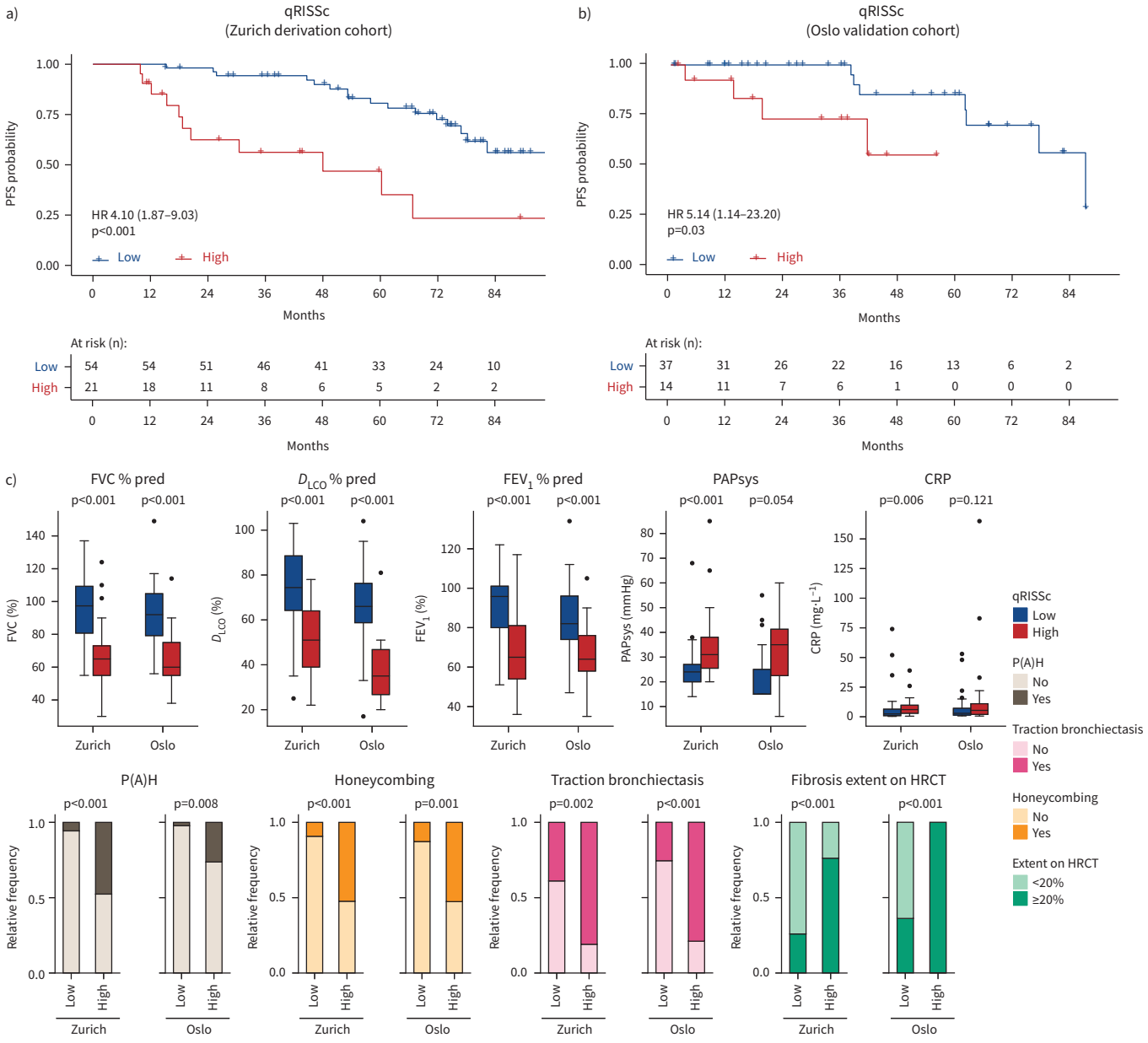

FIGURE 3 Quantitative radiomic risk score (qRISSc)-based risk stratification for future lung function decline and associations of qRISSc with clinical parameters in the derivation and validation cohorts. a, b) Kaplan–Meier curves of the constructed quantitative radiomic interstitial lung disease risk score (qRISSc) for progression-free survival (PFS) defined as time to relative forced vital capacity (FVC) decline ⩾15% in the a) derivation cohort from Zurich and b) external validation cohort from Oslo. Hazard ratio (95% CI) and p-value of the univariate Cox regression are shown. c) Significant associations of qRISSc with clinical parameters in both the derivation (Zurich) cohort and validation (Oslo) cohort. Fisher's exact test was used to compare categorical variables and the Mann–Whitney U-test was used to compare numerical variables. D_{LCO}: diffusing capacity of the lung for carbon monoxide; FEV_1: forced expiratory volume in 1 s; PAPsys: systolic pulmonary arterial pressure; CRP: C-reactive protein; P(A)H: pulmonary (arterial) hypertension; HRCT: high-resolution computed tomography.

datasets, confirming the suitability of this animal model as a pre-clinical "radiomic surrogate" for human ILD (figure 5a).

We then performed pathway enrichment analysis for significantly qRISSc-correlated proteins (634 out of 5311 identified proteins (11.94%) with $\rho \geqslant |0.3|$, $p<0.05$) derived from whole-lung tissue proteomics to reveal associations of qRISSc with molecular pathways and processes related to ILD (figure 5d). We observed that pathways related to fibrosis development, particularly pathways associated with extracellular matrix (ECM) organisation and formation, were most significantly associated with qRISSc (figure 5f and g).

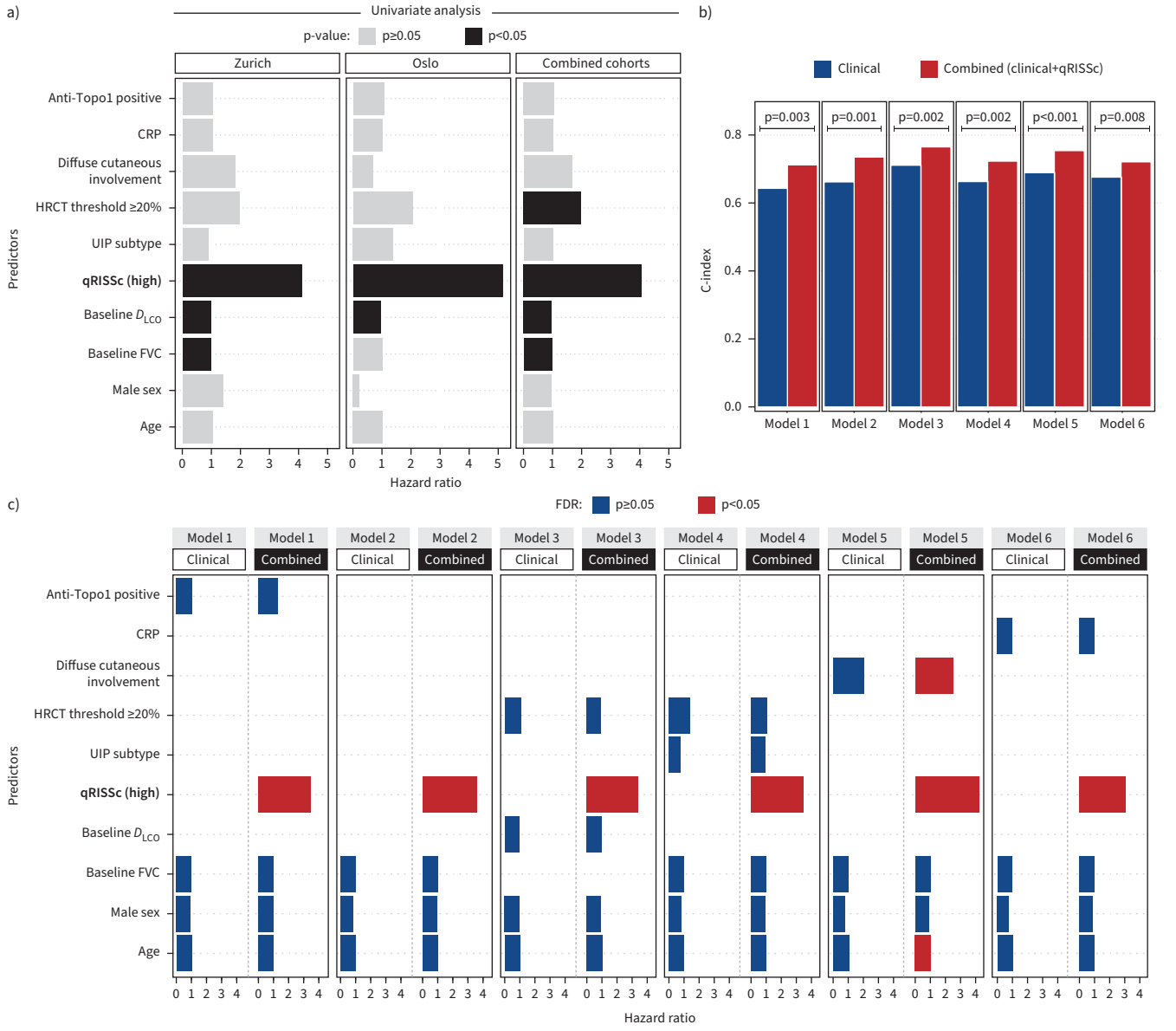

FIGURE 4 Prognostic performance of the quantitative radiomic risk score (qRISSc) compared with other risk factors for systemic sclerosis-associated interstitial lung disease (SSc-ILD) progression. a) Bar plot indicating the results of the univariable Cox regression analysis of qRISSc compared with previously proposed clinical risk factors of SSc-ILD progression. b) Bar plot comparing the predictive power (C-index) of the multivariable models composed of the clinical risk factors of SSc-ILD progression alone (clinical models) *versus* models also incorporating qRISSc (combined models). Two-way ANOVA was used to compare model performances. Model 1: age+male sex+baseline forced vital capacity (FVC) (% pred)+anti-topoisomerase 1 (Topo1)±qRISSc; Model 2: age+male sex+baseline FVC (% pred)±qRISSc; Model 3: age+male sex+baseline diffusing capacity of the lung for oxygen (D_{LCO}) (% pred)+high-resolution computed tomography (HRCT) threshold ⩾20%±qRISSc; Model 4: age+male sex+baseline FVC (% pred)+HRCT threshold ⩾20%+usual interstitial pneumonia (UIP) subtype±qRISSc; Model 5: age+male sex+baseline FVC (% pred)+diffuse cutaneous involvement±qRISSc; Model 6: age+male sex+baseline FVC (% pred)+C-reactive protein (CRP)±qRISSc. Models 1 and 4 (exclusively composed of clinical covariates) were overall not significant. c) Bar plot summarising the false discovery rate (FDR)-corrected results of the multivariable Cox regression analysis incorporating qRISSc (combined models) *versus* multivariable models composed of clinical risk factors alone (clinical models). Bars represent hazard radios for each predictor in each model, whereas colours indicate the p-value of the predictors corrected for multiple testing using the FDR. Covariates for univariable and multivariable Cox regression were selected based on literature evidence [2] and expert opinion.

Consistently, the enriched biological processes that significantly correlated with qRISSc were also linked mainly to pro-fibrotic remodelling processes underlying ILD, including processes related to protein polymerisation and ECM assembly (figure 5e).

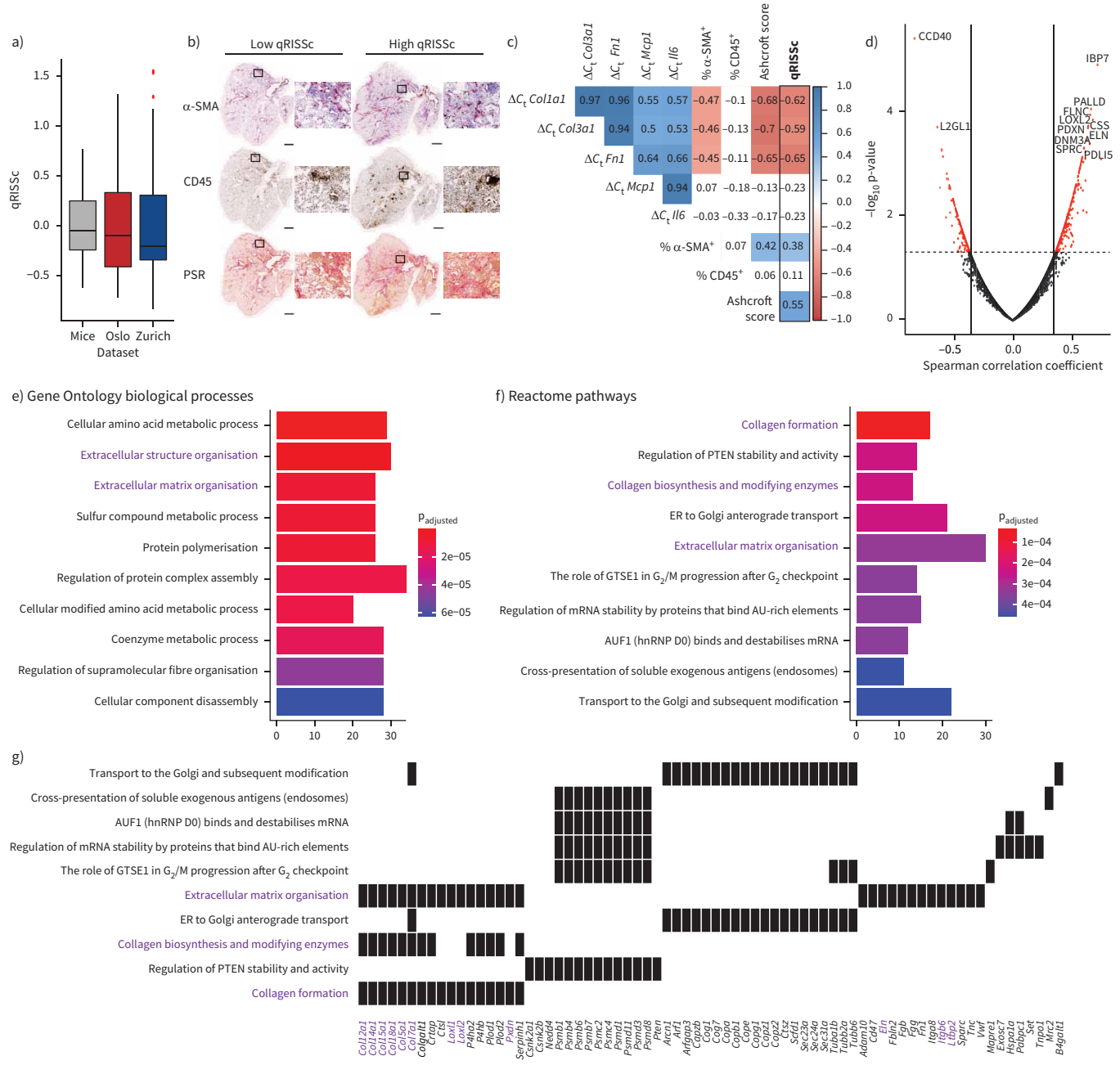

FIGURE 5 Correlation analysis of the quantitative radiomic risk score (qRISSc) with molecular data in experimental interstitial lung disease (ILD). a) Score distribution across the three datasets, demonstrating a similar qRISSc distribution between mice of the bleomycin-induced lung fibrosis model (n=30) and systemic sclerosis-associated ILD (SSc-ILD) patients (Zurich, n=75; Oslo, n=66). b) Representative histological images of bleomycin-treated mice with low and high qRISSc that were stained for the myofibroblast marker α-smooth muscle actin (α-SMA), the pan-leukocyte marker CD45 and picrosirius red (PSR) to visualise collagen fibres (collagen=red). Sections of the entire right caudal lobe (scale bar: 1 mm) with higher magnification views (×100 magnification; scale bar: 100 μm) are shown. c) Correlation matrix for qRISSc with histological parameters (percentage of α-SMA and CD45 positivity, and Ashcroft score), and mRNA expression of inflammatory (*Il6* and *Mcp1*) and fibrotic (*Col1a1*, *Col3a1* and *Fn1*) genes. A lower change in cycle threshold (ΔC_t) value and thus negative correlation indicates higher gene expression. Spearman correlation coefficient ρ is shown. Nonsignificant associations are depicted on a white background. d) Volcano plot for qRISSc-correlated proteins. Proteins with ρ≥|0.3| and p<0.05 are highlighted in red. e) Bar plot of the top 10 (based on p-value) Gene Ontology biological processes associated with qRISSc. f) Bar plot of the top 10 (based on p-value) Reactome pathways associated with qRISSc. g) Heat plot indicating the top enriched proteins per molecular pathway. For (e–g), the most important associations are highlighted in purple. For pathway analyses, only proteins with ρ≥|0.3| and p<0.05 were considered. ER: endoplasmic reticulum; hnRNP: heterogeneous nuclear ribonucleoprotein.

Among the highly and significantly qRISSc-correlated proteins were multiple ECM proteins, such as collagen 5α1 (CO5A1; ρ=0.48), collagen 7α1 (CO7A1; ρ=0.55), collagen 12α1 (COCA1; ρ=0.46), collagen 15α1 (COFA1; ρ=0.48), collagen 18α1 (COIA1; ρ=0.47), filamin-C (FLNC; ρ=0.66) and elastin (ELN; ρ=0.63), as well as proteins required for ECM assembly and cross-linking, including members of the lysyl oxidase family, such as LOXL1 (ρ=0.56) and LOXL2 (ρ=0.68), or peroxidasin (PXDN; ρ=0.64). In addition, proteins involved in transforming growth factor (TGF)-β activation, including latent-TGF-β-binding protein 2 (LTBP2: ρ=0.50) and integrin β6 (ITB6; ρ=0.55), were strongly correlated with qRISSc (figure 5g).

To complement the proteomic analysis, we additionally performed whole-slide digital histopathological and gene expression analysis of established fibrotic and inflammatory markers (figure 5b and c) [38–40]. In line with the proteomic data, qRISSc was also significantly correlated with fibrotic markers on a histological level, with a higher qRISSc value corresponding to a higher fibrosis score (Ashcroft score [41]; ρ=0.55) and increased expression of α-smooth muscle actin, a marker for activated fibroblasts (ρ=0.38). Consistently, qRISSc also showed significant association with the expression of fibrotic genes, including collagen 1α1 (*Col1a1*; ρ=−0.62), collagen 3α1 (*Col3a1*; ρ=−0.59) and fibronectin 1 (*Fn1*; ρ=−0.65), where a lower change in cycle threshold (ΔC_t) value and thus negative correlation indicates higher gene expression. Most notably, on both the histological and gene level, qRISSc was not correlated with inflammatory markers, such as the number of $CD45^+$ inflammatory cells in tissue sections, interleukin-6 (*Il6*) and monocyte chemoattractant protein-1 (*Mcp1*) mRNA expression (figure 5b and c).

Collectively, this demonstrates that qRISSc specifically reflects the underlying fibrotic remodelling processes in experimental ILD, and suggests that fibrotic and not inflammatory pathway activation may be dominant in individuals identified by a high qRISSc score.

Discussion

Herein, we show that radiomics performed on standard-of-care HRCT images provided complementary clinical, prognostic and pathophysiological information with great potential for risk stratification and outcome prediction in SSc-ILD.

Radiomic profiles captured ILD-specific differences based on image intensity, texture and wavelet transformation, and contained prognostic information. Clinical applicability was demonstrated by the accurate prediction of PFS in the combined SSc-ILD cohorts using a newly derived quantitative, binary radiomic risk score for SSc-ILD that can be calculated from a patient's routine HRCT scan. The integration of qRISSc into models composed of previously suggested risk factors [22–30] significantly improved the predictive power measured by the C-index. In all analyses, qRISSc was the strongest (HR 3.07–4.23) and often the only significant predictor in the combined models, thereby underlining the added value of qRISSc.

In both independent study cohorts, "high-risk patients" identified by clustering or risk scoring (qRISSc) were characterised by a more severe ILD phenotype, more compromised lung function, presence of pulmonary hypertension and specific visual ILD HRCT patterns, including honeycombing and traction bronchiectasis, all of which have been discussed as potential risk factors in SSc-ILD [2, 42]. The fact that we did not observe correlations with other suggested clinical risk factors, *e.g.* diffuse cutaneous SSc subset, older age, male sex, anti-topoisomerase 1 positivity [25, 43] or CRP [22], underlines that radiomic features capture lung-specific information independent of demographic and clinicoserological characteristics.

The benefit of radiomics might arise from the integrative and in-depth information obtained on whole-lung pathology, where tissue heterogeneity is reflected on different spatial levels. In radiomic terms, spatial tissue heterogeneity is best described by texture features, which identify different image patterns by describing voxel intensities and their spatial arrangement [44]. In our study, most qRISSc features (*e.g.* "coarseness", "cluster tendency" and "sum of variance") belonged to the class of texture features or of wavelet transformations thereof. Investigating the added value of qRISSc compared with a radiomic score composed only of intensity features further showed that inclusion of such more complex features is crucial for prognostic performance. Our results are in line with previous studies where texture features outperformed first-order (intensity) features for prognostic purposes [8, 10, 15, 33] and where texture features were found to stratify patients according to disease severity [45]. In contrast to deep learning-based models, which require large datasets and represent "black box" approaches without an underlying biological rationale [46], radiomic features were shown to not only correlate with

morphological but also with molecular tissue characteristics. This in-depth information provided by radiomics adds a new dimension to previously developed quantitative image analysis [12–14].

The hypothesis that radiomic features reflect the underlying pathophysiology was supported in our study, where we used a cross-species approach integrating imaging with molecular data to define the biological basis of qRISSc. In experimental ILD, a high qRISSc score was closely linked to specific fibrotic remodelling processes yet did not correlate with inflammation as assessed on a multiscale molecular level. The fibrotic pathway activation tied in with the worse outcome of the high-risk group of SSc-ILD patients identified by qRISSc [47]. The ability of radiomic markers to reflect the entire lung pathology is particularly attractive in a complex multiorgan disease with high molecular heterogeneity such as SSc [48]. The fact that radiomic features, including qRISSc, were reverse translatable from humans to mice demonstrates that well-characterised and representative animal models could prove valuable to test defined hypotheses in radiomics research, particularly for studying links with pathophysiology in rare diseases with low numbers of patients and limited access to biosamples.

Our study has some limitations, which despite the high-quality registry data from two independent, prospectively followed SSc cohorts from academic expert sites [49] mainly arise from the relatively low numbers of patients with this orphan disease. Appropriately, we did not impute missing data since the lack of data could not be assumed random. Furthermore, due to the modest sample size of our derivation cohort, we lacked the power to assess variable importance (measured by LASSO coefficients) and therefore assigned equal importance to each feature following a maximum likelihood approach to construct qRISSc. Notably, despite this fact, we could fit significant multivariable models with good prognostic power on the combined cohort dataset, demonstrating the clinical applicability of our quantitative radiomic risk score (qRISSc) and the potential to support clinical decision making by improving upon existing risk parameters. Future large-scale collaborative studies designed to consider analytical methodologies for high-dimensional data will allow us to determine feature importance, perform proper weighting of score features and evaluate further the added predictive value of radiomic signatures. Other limitations arise from exclusively focusing the analysis on SSc-ILD, which is relatively mild and of different aetiology compared with many other forms of fibrosing ILDs. Since the severity of ILD of the SSc patients included in our study was well in line with recently published data from the EUSTAR cohort [23], we consider our approach to apply to other SSc-ILD cohorts. Whether it applies to more severe forms and different aetiologies of fibrosing ILD, such as idiopathic pulmonary fibrosis, has yet to be determined.

Concerns about the reproducibility of radiomic features arise from their dependency on image acquisition and reconstruction methodologies and the intra-/inter-observer variability during image segmentation [50, 51]. In our study, radiomic features, including qRISSc, proved to be very stable against semiautomated lung segmentation. In addition, no batch effects concerning different CT scanner types, scan and reconstruction protocols across two inhomogeneous cohorts of patients from independent sites occurred. This emphasises the translational potential of our results and is a strong argument for the future clinical application of radiomics. We cannot, however, exclude that the adherence to predefined quality criteria of the HRCT scan settings to ensure comparability between the two cohorts may have led to a specific selection bias of patients.

In conclusion, this work highlights radiomic profiling as a noninvasive means to capture SSc-ILD heterogeneity by decoding clinical and prognostic differences and relaying pathophysiological information. We provide a clinically applicable quantitative risk score for predicting PFS in SSc-ILD, which improves upon conventional risk factors. Whether it also allows the prediction of treatment response will be the subject of future studies.

Acknowledgements: Microscopic image recording was performed with equipment maintained by the Centre for Microscopy and Image Analysis, University of Zurich, Zurich, Switzerland. We acknowledge Maria Comazzi (Centre of Experimental Rheumatology, University Hospital Zurich, Zurich, Switzerland) for her technical assistance with the histological analyses.

Data availability: All data (clinical, radiomic and molecular) and code for reproduction of the main findings of this study will be made publicly available after publication.

Author contributions: J. Schniering contributed to the design and conception of the work, was involved in acquisition, analysis and interpretation of radiomic, clinical and molecular data, and wrote the manuscript. M. Maciukiewicz contributed to the design and conception of the work, performed the statistical

analysis, and drafted the manuscript. M. Brunner contributed to the acquisition and analysis of radiomic, clinical and molecular data, and revised the manuscript. H.S. Gabrys and C. Blüthgen were involved in the acquisition and analysis of radiomic data, and revised the manuscript. S. Braga-Lagache, A-C. Uldry and M. Heller contributed to the acquisition and interpretation of proteomic data, and revised the manuscript. M. Guckenberger contributed to the analysis and interpretation of radiomic and clinical data, and revised the manuscript. C. Meier, H. Fretheim and A-M. Hoffmann-Vold contributed to the acquisition and interpretation of clinical data, and revised the manuscript. C.T. Nakas contributed to the statistical analysis and interpretation of data, and revised the manuscript. O. Distler contributed to the analysis and interpretation of clinical and molecular data, and revised the manuscript. T. Frauenfelder and S. Tanadini-Lang contributed to the acquisition, analysis and interpretation of radiomic data, and revised the manuscript. B. Maurer was central for the design and conception of the work, was involved in acquisition, analysis and interpretation of radiomic, clinical and molecular data, and wrote the manuscript.

Conflict of interest: J. Schniering reports grants from Forschungskredit PostDoc from the University of Zurich, during the conduct of the study. M. Maciukiewicz has nothing to disclose. H.S. Gabrys has nothing to disclose. M. Brunner has nothing to disclose. C. Blüthgen has nothing to disclose. C. Meier reports grants from the Bangerter Foundation and Swiss Academy of Medical Sciences, during the conduct of the study. S. Braga-Lagache has nothing to disclose. A-C. Uldry has nothing to disclose. M. Heller has nothing to disclose. M. Guckenberger has nothing to disclose. H. Fretheim received travel bursaries from Actelion and GSK, and remuneration from Bayer. C.T. Nakas has nothing to disclose. A-M. Hoffmann-Vold had grant/research support from Boehringer Ingelheim and received speaker and personal fees from Boehringer Ingelheim, Roche, Actelion, MSD, Medscape and Bayer. O. Distler had consultancy relationship and/or has received research funding from AbbVie, Actelion, Acceleron Pharma, Amgen, AnaMar, Baecon Discovery, Blade Therapeutics, Bayer, Boehringer Ingelheim, Catenion, Competitive Drug Development International Ltd, CSL Behring, ChemomAb, Curzion Pharmaceuticals, Ergonex, Galapagos NV, Glenmark Pharmaceuticals, GSK, Inventiva, Italfarmaco, iQone, iQvia, Lilly, Medac, Medscape, Mitsubishi Tanabe Pharma, MSD, Novartis, Pfizer, Roche, Sanofi, Target Bio Science and UCB in the area of potential treatments of scleroderma and its complications; and has a patent “mir-29 for the treatment of systemic sclerosis issued” (US8247389, EP2331143). T. Frauenfelder has nothing to disclose. S. Tanadini-Lang has nothing to disclose. B. Maurer reports grants from Gebauer Foundation, Lunge Zürich Foundation, OPO Foundation and Professor Dr Max Cloëtta Foundation, during the conduct of the study; has consultancies with Novartis, Boehringer Ingelheim and Janssen-Cilag, had grant/research support from AbbVie, Protagen, Novartis Biomedical Research, received speaker fees from Boehringer Ingelheim as well as congress support from Medtalk, Pfizer, Roche, Actelion, Mepha, and MSD; and has a patent “mir-29 for the treatment of systemic sclerosis” issued (US8247389, EP2331143).

Support statement: This work was supported by the Forschungskredit PostDoc from the University of Zurich (to J. Schniering; FK-19-046), the Bangerter Foundation and Swiss Academy of Medical Sciences (to C. Meier), as well as the Gebauer Foundation, Lunge Zürich Foundation, OPO Foundation and Professor Dr Max Cloëtta Foundation (to B. Maurer). Funding information for this article has been deposited with the Crossref Funder Registry.

References

1 Hoffmann-Vold A-M, Fretheim H, Halse A-K, *et al.* Tracking impact of interstitial lung disease in systemic sclerosis in a complete nationwide cohort. *Am J Respir Crit Care Med* 2019; 200: 1258–1266.
2 Distler O, Assassi S, Cottin V, *et al.* Predictors of progression in systemic sclerosis patients with interstitial lung disease. *Eur Respir J* 2020; 55: 2002026.
3 Silver KC, Silver RM. Management of systemic-sclerosis-associated interstitial lung disease. *Rheum Dis Clin North Am* 2015; 41: 439–457.
4 Hansell DM, Goldin JG, King TE Jr, *et al.* CT staging and monitoring of fibrotic interstitial lung diseases in clinical practice and treatment trials: a Position Paper from the Fleischner Society. *Lancet Respir Med* 2015; 3: 483–496.
5 Winklehner A, Berger N, Maurer B, *et al.* Screening for interstitial lung disease in systemic sclerosis: the diagnostic accuracy of HRCT image series with high increment and reduced number of slices. *Ann Rheum Dis* 2012; 71: 549–552.
6 Hoffmann-Vold A-M, Aaløkken TM, Lund MB, *et al.* Predictive value of serial high-resolution computed tomography analyses and concurrent lung function tests in systemic sclerosis. *Arthritis Rheumatol* 2015; 67: 2205–2212.
7 Parmar C, Leijenaar RTH, Grossmann P, *et al.* Radiomic feature clusters and prognostic signatures specific for lung and head & neck cancer. *Sci Rep* 2015; 5: 11044.
8 Aerts HJWL, Velazquez ER, Leijenaar RTH, *et al.* Decoding tumour phenotype by noninvasive imaging using a quantitative radiomics approach. *Nat Commun* 2014; 5: 4006.

9 Aerts HJWL, Grossmann P, Tan Y, *et al.* Defining a radiomic response phenotype: a pilot study using targeted therapy in NSCLC. *Sci Rep* 2016; 6: 33860.

10 Lu H, Arshad M, Thornton A, *et al.* A mathematical-descriptor of tumor-mesoscopic-structure from computed-tomography images annotates prognostic- and molecular-phenotypes of epithelial ovarian cancer. *Nat Commun* 2019; 10: 764.

11 Lambin P, Rios-Velazquez E, Leijenaar R, *et al.* Radiomics: extracting more information from medical images using advanced feature analysis. *Eur J Cancer* 2012; 48: 441–446.

12 Tashkin DP, Volkmann ER, Tseng C-H, *et al.* Relationship between quantitative radiographic assessments of interstitial lung disease and physiological and clinical features of systemic sclerosis. *Ann Rheum Dis* 2016; 75: 374–381.

13 Abtin FG, Khanna D, Furst DE, *et al.* Validation of a computer aided quantitative fibrosis score in systemic sclerosis patients. *Am J Respir Crit Care Med* 2010; 181: A2353.

14 Kim HG, Tashkin DP, Clements PJ, *et al.* A computer-aided diagnosis system for quantitative scoring of extent of lung fibrosis in scleroderma patients. *Clin Exp Rheumatol* 2010; 28: S26–S35.

15 Grossmann P, Stringfield O, El-Hachem N, *et al.* Defining the biological basis of radiomic phenotypes in lung cancer. *Elife* 2017; 6: e23421.

16 Minier T, Guiducci S, Bellando-Randone S, *et al.* Preliminary analysis of the Very Early Diagnosis of Systemic Sclerosis (VEDOSS) EUSTAR multicentre study: evidence for puffy fingers as a pivotal sign for suspicion of systemic sclerosis. *Ann Rheum Dis* 2014; 73: 2087–2093.

17 van den Hoogen F, Khanna D, Fransen J, *et al.* 2013 classification criteria for systemic sclerosis: an American College of Rheumatology/European League against Rheumatism collaborative initiative. *Arthritis Rheum* 2013; 65: 2737–2747.

18 LeRoy EC, Black C, Fleischmajer, *et al.* Scleroderma (systemic sclerosis): classification, subsets and pathogenesis. *J Rheumatol* 1988; 15: 202–205.

19 Liu T, De Los Santos FG, Phan SH. The bleomycin model of pulmonary fibrosis. *Methods Mol Biol* 2017; 1627: 27–42.

20 Harrell FE. Regression Modeling Strategies: With Applications to Linear Models, Logistic and Ordinal Regression, and Survival Analysis. Cham, Springer, 2015.

21 Goh NSL, Desai SR, Veeraraghavan S, *et al.* Interstitial lung disease in systemic sclerosis: a simple staging system. *Am J Respir Crit Care Med* 2008; 177: 1248–1254.

22 Wu W, Jordan S, Becker MO, *et al.* Prediction of progression of interstitial lung disease in patients with systemic sclerosis: the SPAR model. *Ann Rheum Dis* 2018; 77: 1326–1332.

23 Hoffmann-Vold A-M, Allanore Y, Alves M, *et al.* Progressive interstitial lung disease in patients with systemic sclerosis-associated interstitial lung disease in the EUSTAR database. *Ann Rheum Dis* 2021; 80: 219–227.

24 Winstone TA, Assayag D, Wilcox PG, *et al.* Predictors of mortality and progression in scleroderma-associated interstitial lung disease: a systematic review. *Chest* 2014; 146: 422–436.

25 Nihtyanova SI, Schreiber BE, Ong VH, *et al.* Prediction of pulmonary complications and long-term survival in systemic sclerosis. *Arthritis Rheumatol* 2014; 66: 1625–1635.

26 Zhang XJ, Bonner A, Hudson M, *et al.* Association of gastroesophageal factors and worsening of forced vital capacity in systemic sclerosis. *J Rheumatol* 2013; 40: 850–858.

27 Savarino E, Bazzica M, Zentilin P, *et al.* Gastroesophageal reflux and pulmonary fibrosis in scleroderma: a study using pH-impedance monitoring. *Am J Respir Crit Care Med* 2009; 179: 408–413.

28 Assassi S, Sharif R, Lasky RE, *et al.* Predictors of interstitial lung disease in early systemic sclerosis: a prospective longitudinal study of the GENISOS cohort. *Arthritis Res Ther* 2010; 12: R166.

29 Plastiras SC, Karadimitrakis SP, Ziakas PD, *et al.* Scleroderma lung: initial forced vital capacity as predictor of pulmonary function decline. *Arthritis Rheum* 2006; 55: 598–602.

30 Morgan C, Knight C, Lunt M, *et al.* Predictors of end stage lung disease in a cohort of patients with scleroderma. *Ann Rheum Dis* 2003; 62: 146–150.

31 Ufuk F, Demirci M, Altinisik G. Quantitative computed tomography assessment for systemic sclerosis-related interstitial lung disease: comparison of different methods. *Eur Radiol* 2020; 30: 4369–4380.

32 Bocchino M, Bruzzese D, D'Alto M, *et al.* Performance of a new quantitative computed tomography index for interstitial lung disease assessment in systemic sclerosis. *Sci Rep* 2019; 9: 9468.

33 Saldana DC, Hague CJ, Murphy D, *et al.* Association of computed tomography densitometry with disease severity, functional decline, and survival in systemic sclerosis-associated interstitial lung disease. *Ann Am Thorac Soc* 2020; 17: 813–820.

34 Ariani A, Silva M, Seletti V, *et al.* Quantitative chest computed tomography is associated with two prediction models of mortality in interstitial lung disease related to systemic sclerosis. *Rheumatology* 2017; 56: 922–927.

35 Rizzo S, Botta F, Raimondi S, *et al.* Radiomics: the facts and the challenges of image analysis. *Eur Radiol Exp* 2018; 2: 36.

36 Gillies RJ, Kinahan PE, Hricak H. Radiomics: images are more than pictures, they are data. *Radiology* 2016; 278: 563–577.

37 Schniering J, Gabrys H, Brunner M, *et al.* Computed-tomography-based radiomics features for staging of interstitial lung disease – transferability from experimental to human lung fibrosis – a proof-of-concept study. *Eur Respir J* 2019; 54: Suppl. 63, PA4806.

38 Schniering J, Benešová M, Brunner M, *et al.* F-AzaFol for detection of folate receptor-β positive macrophages in experimental interstitial lung disease – a proof-of-concept study. *Front Immunol* 2019; 10: 2724.

39 Schniering J, Benešová M, Brunner M, *et al.* Visualisation of interstitial lung disease by molecular imaging of integrin αvβ3 and somatostatin receptor 2. *Ann Rheum Dis* 2019; 78: 218–227.

40 Schniering J, Guo L, Brunner M, *et al.* Evaluation of ^{99m}Tc-rhAnnexin V-128 SPECT/CT as a diagnostic tool for early stages of interstitial lung disease associated with systemic sclerosis. *Arthritis Res Ther* 2018; 20: 183.

41 Ashcroft T, Simpson JM, Timbrell V. Simple method of estimating severity of pulmonary fibrosis on a numerical scale. *J Clin Pathol* 1988; 41: 467–470.

42 Perelas A, Silver RM, Arrossi AV, *et al.* Systemic sclerosis-associated interstitial lung disease. *Lancet Respir Med* 2020; 8: 304–320.

43 Walker UA, Tyndall A, Czirjak L, *et al.* Clinical risk assessment of organ manifestations in systemic sclerosis: a report from the EULAR Scleroderma Trials And Research group database. *Ann Rheum Dis* 2007; 66: 754–763.

44 Zwanenburg A, Vallières M, Abdalah MA, *et al.* The image biomarker standardization initiative: standardized quantitative radiomics for high-throughput image-based phenotyping. *Radiology* 2020; 295: 328–338.

45 Martini K, Baessler B, Bogowicz M, *et al.* Applicability of radiomics in interstitial lung disease associated with systemic sclerosis: proof of concept. *Eur Radiol* 2021; 31: 1987–1998.

46 Walsh SLF, Calandriello L, Silva M, *et al.* Deep learning for classifying fibrotic lung disease on high-resolution computed tomography: a case-cohort study. *Lancet Respir Med* 2018; 6: 837–845.

47 Khanna D, Tashkin DP, Denton CP, *et al.* Ongoing clinical trials and treatment options for patients with systemic sclerosis-associated interstitial lung disease. *Rheumatology* 2019; 58: 567–579.

48 Martyanov V, Whitfield ML. Molecular stratification and precision medicine in systemic sclerosis from genomic and proteomic data. *Curr Opin Rheumatol* 2016; 28: 83–88.

49 Meier FMP, Frommer KW, Dinser R, *et al.* Update on the profile of the EUSTAR cohort: an analysis of the EULAR Scleroderma Trials and Research group database. *Ann Rheum Dis* 2012; 71: 1355–1360.

50 Kumar V, Gu Y, Basu S, *et al.* Radiomics: the process and the challenges. *Magn Reson Imaging* 2012; 30: 1234–1248.

51 Yip SSF, Aerts HJWL. Applications and limitations of radiomics. *Phys Med Biol* 2016; 61: R150–R166.